Ann. For. Res. 66(2): 159-172, 2023
ISSN: 18448135, 20652445
ANNALS OF FOREST RESEARCH
www.e-afr.org

SARS-COV-2 INHIBITION BY GINGER EXTRACTION: THEORETICAL AND MODELING STUDIES

Alaa Hamid Faisal [1,2], Mohamed Bouaziz[1], Mohamed Masmoudi[1,3]
[1]Laboratory of Electrochemistry and Environment (LEE), Sfax National Engineering School (ENIS) BPW, 3038 Sfax, University of Sfax, Tunisia.
[2]Department of Pharmacy, Kut University College, AL Kut, Wasit, Iraq 52001.
[3]Preparatory Institute for Engineering Studies of Sfax, BP 805, 3018, University of Sfax, Tunisia.
Corresponding author: Alaa Hamid Faisal; Email: Alaa.Hamid955@gmail.com

Abstract

In the current study, Shogoals (E)-1-(4-Hydroxy-3-methoxyphenyl) dec-4-en-3-one) (1), a chemical derived from ginger, was examined for its potential to suppress SARS-Cov-2. The interaction of extracted chemicals with the spikes on the virus may prevent the virus from replicating or give the immune system time to recognize the virus and produce effective antibodies. Software such as LigPlus, UCA FUKUI, MGL tools, and Gaussian 09 with a 6-311G (d, p) basis set were used. Utilizing the Total Electron Density (TED), FUKUI function, and Millikan charges, the active locations for adsorption were found. Furthermore, docking studies demonstrated unequivocally that binding energy (Eb) and ligand efficiency (LE) are required for the prevention of viral propagation. Docking analysis demonstrated the examined compound's potential to inhibit SARS-CoV-2.

Keywords: SARS-CoV-2, Ginger, Docking, Binding Energy**,** TED

Introduction

Natural cures for many illnesses have become increasingly popular as people's lifestyles change throughout time. Due to their less negative side effects, people choose natural products to synthetic ones all over the world. People are increasingly turning to natural medicines for therapeutic purposes as they become more health-conscious and worried about nutrition.

A popular herbal plant called ginger (Zingiber officinale) is a good choice because of the high concentration of its physiologically active ingredients. It is an effective antioxidant with little drawbacks or adverse effects [1]. Also, it aids in the free radicals scavenging and the lowering of oxidative stressors in the body.

Ginger rhizomes are containing very important chemical constituents which are volatile oils and non-volatile pungent compounds [2]. Terpenoids are the main volatile compounds, while the volatile ones include paradol, zingerone, gingerol, and shagoal.

The fundamental features of ginger mainly belong to the zingerone which is a major flavor component. Zingerone may assist in fighting against a variety of severe illnesses. It also increases respiratory burst, stimulates the immune system [3,4], phagocytic activity, resistance to infections, an excellent appetizer, consequently aiding in the development and maintenance of the body. Further, it possesses anti-inflammatory effects [5], can serve as a hepatoprotective agent [6],

inhibits inflammatory mediators, reduces inflammation and toxicity, and thus can treat a wide range of inflammatory issues of a wide range of diseases. So, because of that many effects, zingerone has been thoroughly investigated, and sure there will be a future need for additional research on the medicinal properties of this natural molecule. Nonetheless, all of the zingerone's known metabolic activities may provide fresh insights into using this amazing natural chemical in therapy to avoid the adverse effects of synthetic medications.

Gingerols and shagoals are other important bioactive components of ginger. According to the previous studies, shagoals were produced by the dehydration of gingerols. It is also found that the conversion of gingerols to shogaols was affected by different drying temperatures and times [7]. It is worth to be mentioned that gingerols are found in higher concentrations than shogoals, but shogoals exhibited higher biological activities including anticancer and antioxidant ones [8, 9].

It is also thought that both gingerol and shagoals are potentially valuable in inducing weight loss because they activate transient receptor potential vanilloid-1 (TRPV1) [2, 10]. In this context, they may be analogous to capsaicin, a compound found in chili peppers with different pharmacological and physiological effects such as; anticancer, antioxidant, and anti-obesity.

For more than two years, the world is facing a major health threat, namely COVID-19. The pandemic was caused by the SARS-CoV-2 virus, first identified in Wuhan, China [11]. The number of positive cases continues to grow every day, and it is predicted to grow over time. With this crisis, there is urgent to develop an agent to prevent or at least reduce the COVID-19 outbreak. Spike (S) is one of the SARS-CoV2 proteins involved in viral entry during infection. They target the host cell's (ACE2) Angiotensin-Converting Enzyme 2 receptor, creating a conducive environment for viral replication. Due to its importance, many drug developments have targeted S protein to prevent disease [12, 13].

Natural-derived compounds are gaining recognition as a potential therapeutic option for various diseases, including viral infection. Herbal research is underway intending to decrease sickness caused by coronavirus [14, 15].

Because of this, the current study was created to look into Ginger's antiviral abilities and the potential for preventing SARS-CoV-2 infection based on ligand interaction with the spike proteins. Using docking calculations on the S protein, an in-silico test for active substances in the ginger was conducted, and the results showed that the tested compounds had good activity. Therefore, based on the research conducted, we believe that a number of active components in ginger may prevent the ACE2 receptor from interacting with the S protein.

Calculations Models

A Becke three-parameter hybrid function and density functional theory (DFT) were employed in the current investigation. Gaussian 09 software was used to do the quantum chemistry calculations utilizing the Lee, Yang, and Parr (B3LYP) model. The 6-311G (d, p) basis set was chosen because it accurately depicts the examined compound's electrical characteristics and geometries in Figure 1 [16]. To derive the protein structure, RCSB (Research Collaboratory for

Structural Bioinformatics) [17] is utilized. The Autodock computations were performed using Molecular Graphic Laboratory (MGL) tools [18, 19]. The Autodock technique (ADT, version 1.5.6) was used to separate the coordinates of the spike structure and ligand. By include all hydrogen atoms and Gasteiger charges, the SARS-CoV-2 spike glycoprotein-S1 and ligand structures were transformed into a format recognized by the ADT (*. pdbqt files) [20]. Unless the user indicates otherwise, the Autodock regularly tries to find the molecule's root, therefore it chooses the root on its own. All ligand atoms' electrostatic, desolation, and atom-specific affinity maps were computed using the auto grid (version 4.2.6). In the gas phase before docking calculations, ligands were tuned. Using the existing DFT approach, the molecular electrostatic potential (TED) and Fukui function were studied [21, 22].

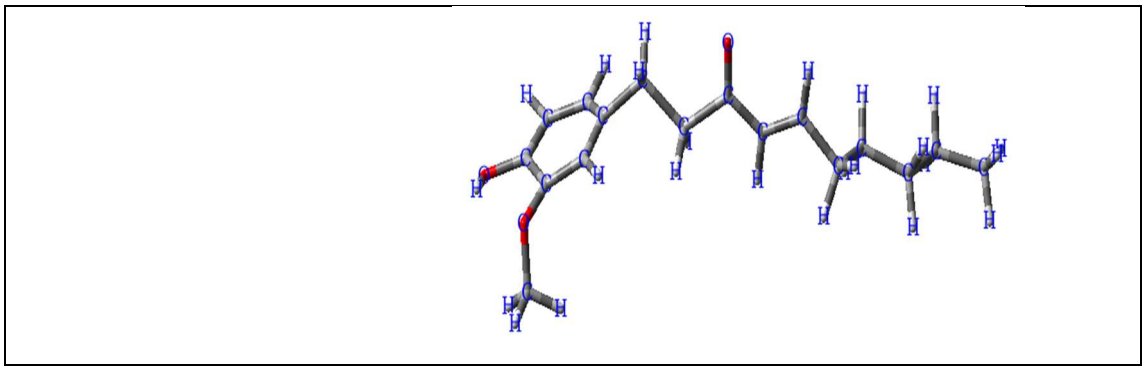

Figure 1: 2D and 3D structures of the studied compound.

Activity and molecular orbitals

This section looks into a few physical characteristics that are linked to the action of the substances under study (23, 24). Regarding ELUMO, a high activity is indicated by a low value for this factor. The discrepancy in energy between HOMO and LUMO orbitals is known as the energy gap. The term "electronegativity" (**χ**) describes an atom's capacity to draw shared electrons. The activity increases as (**ω**) decreases. The Hardness (**η**), the second derivative of E, represents the stability and reactivity of the molecule. The global softness (s), which is a crucial feature for determining molecule stability and reactivity, is the inverse of the global hardness (**σ**). The high activity is inversely correlated with the high value of the dipole moment (**μ**). The investigated parameters for the investigated chemical are shown in Table 1:

The parameters equations are:

$$IE = -E_{HOMO} \quad \text{..... (1)}$$

$$EA = -E_{LUMO} \quad \text{..... (2)}$$

$$\eta = \frac{IE-EA}{2} \quad \text{..... (3)}$$

$$\sigma = \frac{1}{\eta} \quad \text{..... (4)}$$

$$X = \frac{IE+EA}{2} \quad \text{..... (5)}$$

Table 1: Calculated E_{HOMO}, E_{LUMO}, energy bandgap (EH – EL), chemical potential (μ), electronegativity (χ), global hardness (η), global electrophilicity index (ω) and softness (σ) for compound.

EH / eV	EL / eV	(EL-EH) /Ev	χ / eV	μ / eV	η / eV	σ / eV-1	ω / eV	Electroni Energy	Dipole Moment
-5.8118	-1.7619	3.6498	3.5368	-3.5369	1.2749	0.6063	3.9740	-884.057	4.7877

The active sites on the molecules

Figure 2 shows the optimized geometries of the studied molecule analyzed in the gas phase, including LUMO and HOMO density distributions. Red regions represent the ones with high electron density, while the green ones represent low electron density regions [25]. A region with a high electron density (red regions) is the one in which electrons are donated to the receptor (green regions). The electron density of the donor atoms determines the strength of the adsorption bond formed.

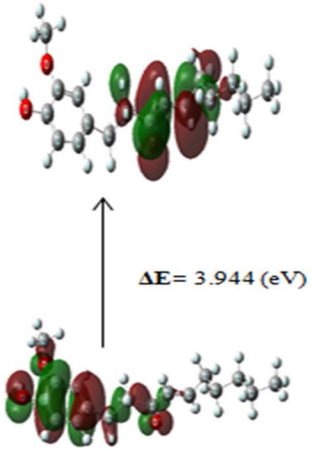

Figure 2: The molecular orbitals (HOMO-LUMO) of the compound.

Total electron density (TED) was used to represent the density of electrons on the molecule. In **Figure 3**, red regions referees to high electron negativity atoms in the studied molecules, such as the oxygen atom, which can promote the nucleophilic attack. Atoms that have moderate electronegativity have been labeled with yellow color. While the blue color regions refer to the atoms that have the highest electro positivity, which enables them to accept the electrons from the donors [26].

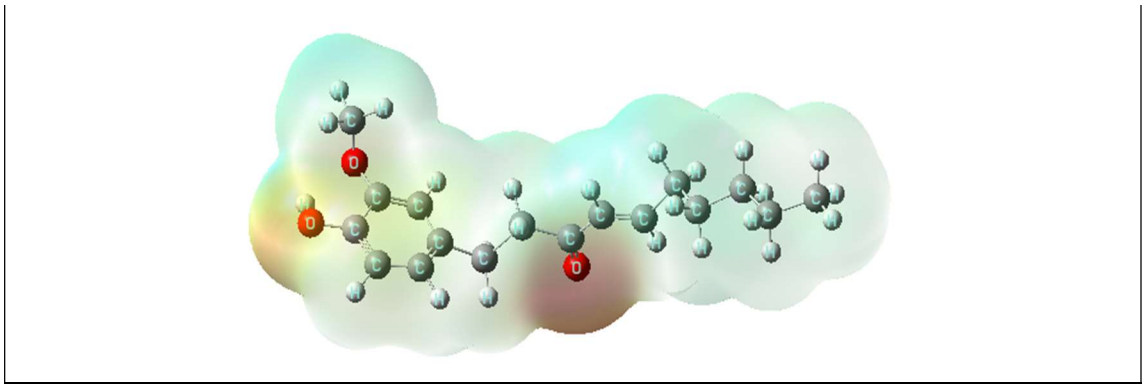

Figure 3: Electron distribution according to TED map.

Electrophilic and nucleophilic attack

The Fukui function (fx) is the derivative of the electronic density in terms of the number of electrons N at a constant external potential, that may be used to identify the most active sites in functional groups of optimal structures. Depending on the electron transfer direction, the Fukui functions [26-29] are obtained using finite difference approximations derived from population analysis of atoms in molecules or compounds. The Fukui and Dual descriptor (D.D) were computed using the DFT technique with basis set (6-311G/d, p), using Gaussian 09 and USA FUKUI software. Table 2 shows that (f+) represents the ability to accept an electron, and (f-) represents the ability to donate an electron. We can distinguish between electrophilic (+) and nucleophilic (-) atoms using Dual Descriptor. The more electrophilic atoms were C7, C6, H28, and H32 for compound 1, and C10, C12, O14, H24, and H28 for compound 2, and C3, C4, and H22 for compound 1.

DFT technique was used in the investigation of the reactive (nucleophilic and electrophilic) centers on the studied molecules. The electron density is vital for estimating chemical reactivity, hence the large electronic charge regions on the molecule are softer than the small electronic charge ones. The electrical charges on the molecules cause electrostatic interactions. Charges affect the physicochemical characteristics of the reactions [30,31], hence the determination of the electrophilic attack site (**Figure 4**). The Millikan charge authorized FUKUI.

Table 2: FUKUI function and dual descriptor of the studied compounds.

Atom	f+	f-	D.D
C1	0.0096	0.0062	0.0034
C2	0.0052	0.0192	0.0140-
C3	0.1536	0.0076	0.1460

C4	0.1191	0.0119	0.1072
C5	0.3876	0.0025	0.3851
C6	0.0063	0.0003	0.0060
C7	0.0531	0.0000	0.0531
C8	0.0100	0.0000	0.0100
C9	0.0004	0.0000	0.0004
C10	0.0010	0.0000	0.0010
O11	0.1683	0.0152	0.1531
C12	0.0083	0.0827	0.0744-
C13	0.0090	0.0149	0.0059-
C14	0.0014	0.0604	0.0590-
C15	0.0004	0.0748	0.0744-
C16	0.0009	0.0381	0.0372-
C17	0.0017	0.0286	0.0270-
O18	0.0001	0.0128	0.0127-
C19	0.0000	0.0069	0.0068-
O20	0.0001	0.0990	0.0989-
H21	0.0014	0.0024	0.0010-
H22	0.0033	0.0015	0.0018
H23	0.0064	0.0001	0.0064

H24	0.0302	0.0000	0.0302
H25	0.0003	0.0001	0.0002
H26	0.0025	0.0001	0.0024
H27	0.0063	0.0000	0.0062
H28	0.0059	0.0000	0.0059
H29	0.0007	0.0000	0.0007
H30	0.0016	0.0000	0.0016
H31	0.0008	0.0000	0.0008
H32	0.0002	0.0000	0.0002
H33	0.0000	0.0000	0.0000
H34	0.0005	0.0000	0.0005
H35	0.0003	0.0000	0.0003
H36	0.0000	0.0000	0.0000
H37	0.0000	0.0000	0.0000
H38	0.0002	0.0008	0.0005-
H39	0.0000	0.0003	0.0003-
H40	0.0000	0.0001	0.0000
H41	0.0000	0.0000	0.0000
H42	0.0000	0.0003	0.0003-
H43	0.0000	0.0004	0.0004-

H44	0.0032	0.5129	0.5096-

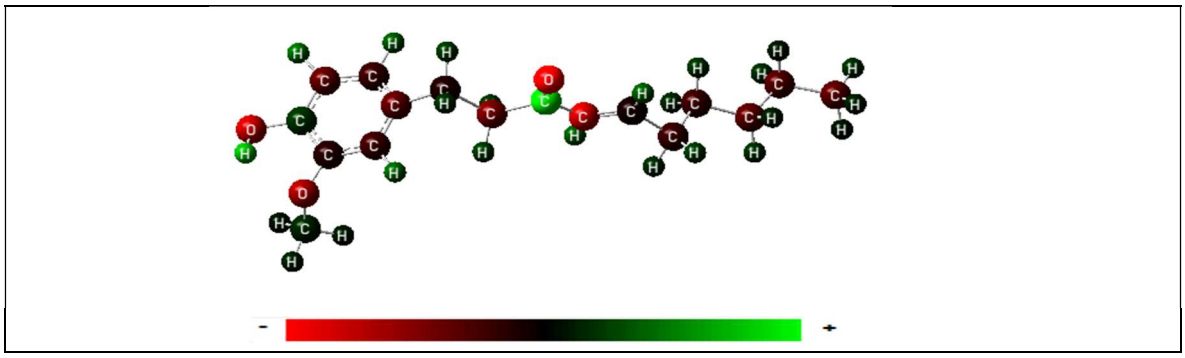

Figure 4: Distribution of Millikan charges on compound structure.

Interaction of inhibitors with the virus spikes

The interaction of compound 1 with the spikes is thought to be the mechanism of SARS-CoV-2 virus suppression, which might improve the immune system involvement. According to geometry optimization, the active functional groups in the proposed inhibitions are OH and C=O. There is planarity in some parts (according to cis and trans of atoms in the molecule, the dihedral angle of each four cis atoms is near to zero, while in trans is near to 180°).

The structure code (6acd) of the spikes downloaded by PDB is shown in **Figure 5**, along with the interaction of ginger active compound 1 with the protein virus. The best active sites for connecting with the protein were compared by measuring the binding energy or the affinity of inhibitors to the receptor [32, 33]. The root means square deviation (RMSD) of the studied compound 9.51. The range of binding energy (kcal/mol) was -1.92 to -3.45. The binding energy (kcal/mol) -3.45, (**Table 3**).

Furthermore, the Ligand Efficiency (LE) per atom in the ligand to the receptor protein is -0.17 kcal/mol [34, 35]. Depending on the above-mentioned results, the body may have adequate time to develop appropriate antibodies that may be resistant to the targeted virus.

Table 3: Binding energy values and ligand efficiency of the studied compounds.

Eb (kcal/mol)	LE	Eb range	Best site number	RMSD
-3.75	-0.19	-1.92 to -3.75	9	9.41

The active sites that accept and donate hydrogen bonds for the receptor are shown in **Figure 6**. The hydrophilic and hydrophobic properties of the materials depend on their affinity to contact or repel water molecules. In **Figure 7**, blue color regions refer to the more negative ones (hydrophilic), whereas the red color regions refer to the more positive ones (hydrophobic).

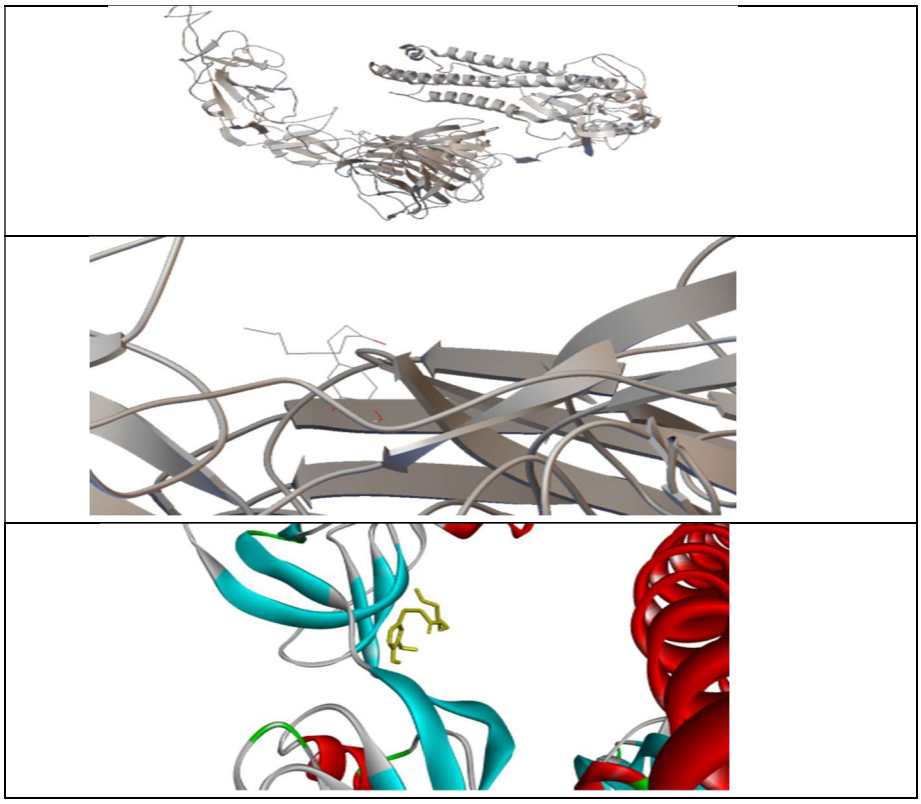

Figure 5: Protein structure with compounds 1.

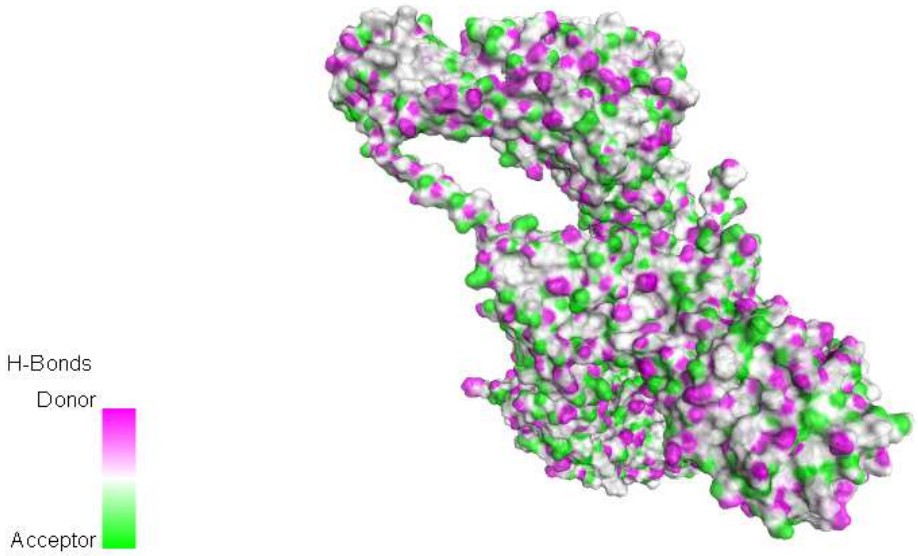

Figure 6: H-bond donor and acceptor sites on the spikes structure**.**

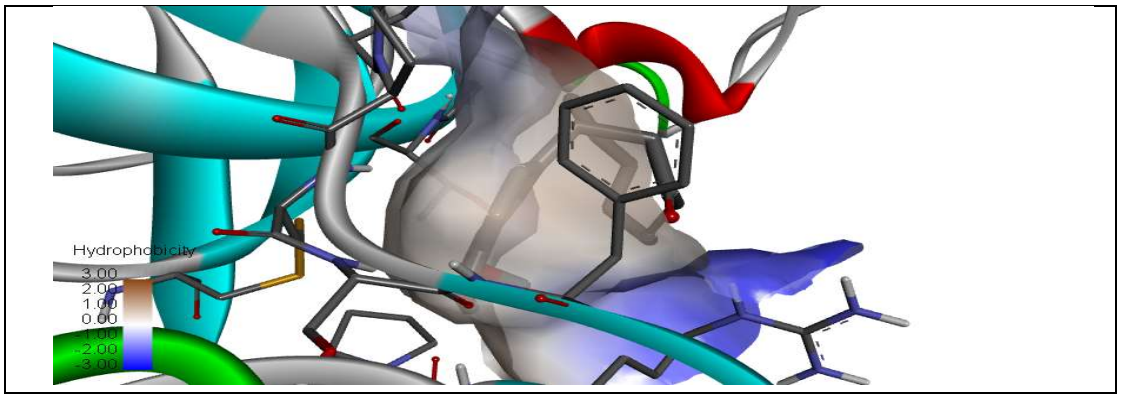

Figure 7: Hydrophilic and hydrophobic sites in the linkage area of inhibitors and spikes.

The bonds of inhibitors with virus's amino acids

Analyzing the results from the DSV, LigPlus, and MGL tools, as shown in Figure 8, highlights the interaction between the viral spikes' amino acids and the suggested inhibitor. Tyrosine-C-H interaction (TYR) is the inhibitor. Additionally, compound 1 showed three different kinds of interactions with protein spikes, including hydrogen bonds between Serine (SER), Valine (VAL), and Arginine (ARG). The amino acids Proline (PRO) and Cysteine (CYS) also interact with the pi electrons of the aromatic ring via alkyl and pi-alkyl interactions. ARG-Ocompound 1 and VAL-Ocompound 1 have hydrogen bonds that are 3.12 and 2.86 long, respectively (Figure 5).

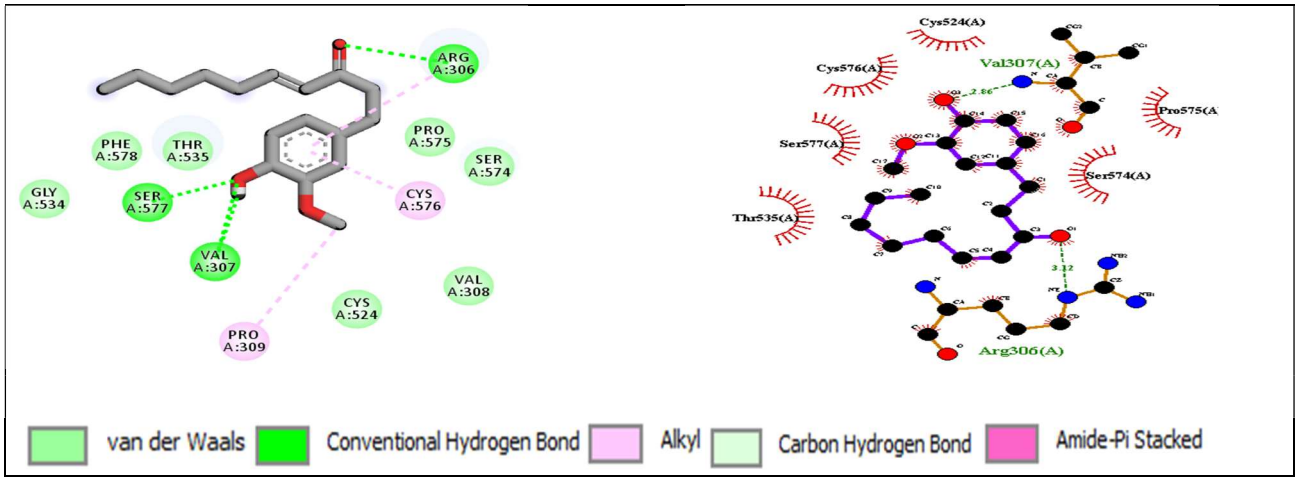

Figure 8: 2D structure of inhibitor and amino acids spikes.

Acknowledgments

The authors acknowledge the facilities from their Universities.

Conclusion

The theoretical analysis of ginger active compound 1's suppression of the SARS-CoV-2 virus. Computational research was done to examine how the potential inhibitors would interact with the spikes of the virus. It was discovered that the OH and C=O groups were utilized as

inhibitors in the interaction between the virus spikes' protein and the inhibitors. To forecast the electron density on the atoms of suggested inhibitors, Dual Descriptor was utilized to discriminate between electrophilic (+) and nucleophilic (-) atoms. The Mulliken charges that were generated agreed well with the FUKUI function. The binding energy showed the spike proteins' high affinity for the active ingredients in ginger. Calculations show that the investigated chemical 1, alkyl, and pi-alkyl interactions with the spikes.

References

1. Addel-Gaber AM, Abd-El-Nabey BA, Sidahmed IM, El-Zayady AM, Saadawy M (2006) Kinetics and thermodynamics of aluminum dissolution in 1.0 M sulphuric acid containing chloride ions. Mater Chem Phys 98:291–297.

2. Mayumi Okamoto, Hiroyuki Irii, Yu Tahara, Hiroyuki Ishii, Akiko Hirao, Haruhide Udagawa, Masaki Hiramoto, Kazuki Yasuda, Atsuo Takanishi, Shigenobu Shibata, and Isao Shimizu. Synthesis of a New [6]-Gingerol Analogue and Its Protective Effect concerning the Development of Metabolic Syndrome in Mice Fed a High-Fat Diet, J. Med. Chem., 2011, 54, 6295-6304.

3. Domingue L, Fernandes JCS (2003) Anodising of Al 2024-T3 in a modifed sulphuric acid/boric acid bath for aeronautical applications. Corros Sci 45:149–160.

4. Gerengi, H.; Darowicki, K.; Bereket, G.; Slepski, P. Evaluation of corrosion inhibition of brass-118 alloy in artificial seawater by benzotriazole using dynamic EIS. Corros. Sci. 2009, 51, 2573.

5. Dunya Edan AL-Mammar Rawaa Abbas Mohammed, Using natural materials as corrosion inhibitors for carbon-steel on phosphoric acid medium, Iraqi Journal of Science 60 (Special Issue), 40-45.

6.Almashhdani, H.A., Al-Saadie, K.A., Corrosion Protection of Carbon Steel in seawater by alumina nanoparticles with poly (acrylic acid) as charging agent, Moroccan Journal of Chemistry, 2018, 6(3), pp. 455–465.

7.Apprael S. Y., Anees A. Khadom and Rafal K. W. (2014) Garlic Powder as a Safe Environment Green Corrosion Inhibitor for Mild Steel in Acidic Media; Adsorption and Quantum Chemical Studies, J. Chin. Chem. Soc., 61:615-623.

8. Fadhil, Ahmed A., Anees A. Khadom, Salima K. Ahmed, Hongfang Liu, Chaoyang Fu, and Hameed B. Mahood. "Portulaca grandiflora as new green corrosion inhibitor for mild steel protection in hydrochloric acid: Quantitative, electrochemical, surface and spectroscopic investigations." *Surfaces and Interfaces* 20 (2020): 100595.

9.Baker M. A., Ramy M. A., Anees A. Kh. and Firas H. K. (2019) Experimental and Theoretical Studies for Tobacco Leaf Extract as an Eco-friendly Inhibitor for Steel in Saline Water, Journal of Bio- and Tribo-Corrosion, 5:75

10. Abolaji, A.O.; Ojo, M.; Afolabi, T.T.; Arowoogun, M.D.; Nwawolor, D.; Farombi, E.O. Protective properties of 6-gingerol-rich fraction from Zingiber o_cinale (ginger) on chlorpyrifos-

induced oxidative damage and inflammation in the brain, ovary, and uterus of rats. Chem. Biol. Interact. **2017**, 270, 15–23

11. Ji, K.; Fang, L.; Zhao, H.; Li, Q.; Shi, Y.; Xu, C.; Wang, Y.; Du, L.; Wang, J.; Liu, Q. Ginger oleoresin alleviated gamma-ray irradiation-induced reactive oxygen species via the Nrf2 protective response in human mesenchymal stem cells. Oxid. Med. Cell. Longev. 2017, 2017, 1480294.

12. Abolaji, A.O.; Ojo, M.; Afolabi, T.T.; Arowoogun, M.D.; Nwawolor, D.; Farombi, E.O. Protective properties of 6-gingerol-rich fraction from Zingiber o_cinale (ginger) on chlorpyrifos-induced oxidative damage and inflammation in the brain, ovary, and uterus of rats. Chem. Biol. Interact. **2017**, 270, 15–23

13. Zhang, G.; Nitteranon, V.; Chan, L.Y.; Parkin, K.L. Glutathione conjugation attenuates biological activities of 6-dehydroshogaol from ginger. Food Chem. 2013, 140, 1–8.

14. Moon, Y.; Lee, H.; Lee, S. Inhibitory e ects of three monoterpenes from ginger essential oil on growth and aflatoxin production of Aspergillus flavus and their gene regulation in aflatoxin biosynthesis. Appl. Biol. Chem.2018, 61, 243–250.

15. Suk, S.; Kwon, G.T.; Lee, E.; Jang, W.J.; Yang, H.; Kim, J.H.; Thimmegowda, N.R.; Chung, M.; Kwon, J.Y.; Yang, S.; et al. Gingerenone A, a polyphenol present in ginger, suppresses obesity and adipose tissue inflammation in high-fat diet-fed mice. Mol. Nutr. Food Res. 2017, 61, 1700139.

16. Noor Ali Khudhair, Mustafa M. Kadhim, and Anees A. Khadom 2021 "Effect of Trimethoprim drug dose on corrosion behavior of stainless steel in simulated human body Environment: Experimental and theoretical investigations", Bio- and Tribo-Corrosion, 7(124), 1-15

17. C. Yu, R. Chen, J.J. Li, J.J. Li, M. Drahansky, M.. Paridah, A. Moradbak, A.. Mohamed, H. abdulwahab taiwo Owolabi, FolaLi, M. Asniza, S.H. Abdul Khalid, T. Sharma, N. Dohare, M. Kumari, U.K. Singh, A.B. Khan, M.S. Borse, R. Patel, A. Paez, A. Howe, D. Goldschmidt, C. Corporation, J. Coates, F. Reading, We are IntechOpen, the world's leading publisher of Open Access books Built by scientists, for scientists TOP 1 %, Intech. (2012) 13. https://doi.org/10.1016/j.colsurfa.2011.12.014.
(2020) 104694. https://doi.org/10.1016/j.fitote.2020.104694.

18. K. Sayin, S.E. Kariper, M. Taştan, T.A. Sayin, D. Karakaş, Investigations of structural, spectral, electronic, and biological properties of N-heterocyclic carbene Ag(I) and Pd(II) complexes, J. Mol. Struct. 1176 (2019) 478–487. https://doi.org/10.1016/j.molstruc.2018.08.103.

19. A.M. Zimmermann-klemd, J.K. Reinhardt, T. Nilsu, A. Morath, C.M. Falanga, W.W. Schamel, R. Huber, M. Hamburger, Fitoterapia Boswellia carteri extract and 3- O -acetyl-alpha-boswellic acid suppress T cell function, Fitoterapia. 146 (2020) 104694. https://doi.org/10.1016/j.fitote.2020.104694.

20. J.Q. Yu, Y.L. Geng, D.J. Wang, H.W. Zhao, L. Guo, X. Wang, Terpenes from the gum resin of Boswellia carterii and their NO inhibitory activities, Phytochem. Lett. 28 (2018) 59–63.

https://doi.org/10.1016/j.phytol.2018.09.010.
21. B. AD, No TitleDensity-functional thermochemistry. III. The role of exact exchange, J. Chem. Phys. 98 (1993) 5648–5652.
22. C. Lee, W. Yang, R.G. Parr, Development of the Colle-Salvetti correlation-energy formula into a functional of the electron density, Phys. Rev. B. 37 (1988) 785–789.
23. Yaqo EA, Annee RA, Abdulmajeed MH, Tomi IH, Kadhim MM. Aminotriazole Derivative as Anti-Corrosion Material for Iraqi Kerosene Tanks: Electrochemical, Computational, and the Surface Study. Chemistry Select 2019; 4(34): 9883- 9892.
24. Mustafa M. Kadhim and Rehab M. Kubba (2020), "Theoretical Investigation on Reaction Pathway, Biological Activity, Toxicity and NLO Properties of Diclofenac Drug and Its Ionic Carriers", Iraqi Journal Kadhim and Kubba of Science, Vol. 61, No. 5, pp: 936-951
25. Ahmed H. Radhi, Ennas AB. Du, Fatma A. Khazaal, Zaid M. Abbas, Oday H. Aljelawi, Salam D. Hamadan, Haider A. Almashhadani and Mustafa M. Kadhim, 2020, HOMO-LUMO Energies and Geometrical Structures Effect on Corrosion Inhibition for Organic Compounds Predict by DFT and PM3 Methods, NeuroQuantology | January 2020 | Volume 18 | Issue 1 | Page 37-45.
26. M.M. Kadhim, R.M. Kubba, "Theoretical Investigation on Reaction Pathway, Biological Activity, Toxicity and NLO Properties of Diclofenac Drug and Its Ionic Carriers" J B U, (2020) 61 951 –936. https://doi.org/10.24996/ijs.2020.61.5.1.
26. D.R. Koes, M.P. Baumgartner, C.J. Camacho, Lessons learned in empirical scoring with smina from the CSAR 2011 benchmarking exercise, J. Chem. Inf. Model. 53 (2013) 1893–1904. https://doi.org/10.1021/ci300604z.
27. Æ. Frisch, R.E. Plata, D.A. Singleton, Gaussian 09W Reference, J. Am. Chem. Soc. 137 (2009) 3811–3826. https://doi.org/10.1021/ja5111392.
28. H. Li, K.S. Leung, P.J. Ballester, M.H. Wong, Istar: A web platform for large-scale protein-ligand docking, PLoS One. 9 (2014). https://doi.org/10.1371/journal.pone.0085678.
29. T.A. Yousef, A.I.A. Al-nassiry, Antimicrobial, computational, and molecular docking studies of Zn (II) and Pd (II) complexes derived from piperidine dithiocarbamate, (2020) 1–15. https://doi.org/10.1002/aoc.6108.
30. Abdul E, Fanfoon DY, Al-uqaily RAH, et al. Materials Today: Proceedings 1-Isoquinolinyl phenyl ketone as a corrosion inhibitor: A theoretical study. Mater Today Proc. 2021. Volume 42, Part 5, 2021, Pages 2241-2246, doi:10.1016/j.matpr.2020.12.310
31. Eva A. Y., Rana A. A., Majid H. A., Ivan H. R. and Mustafa M. K. (2019) Electrochemical, morphological and theoretical studies of an oxadiazole derivative as an anti-corrosive agent for kerosene reservoirs in Iraqi refineries, Chemical Papers, 4:9883-9892
32. H. Li, K.S. Leung, P.J. Ballester, M.H. Wong, Istar: A web platform for large-scale protein-ligand docking, PLoS One. 9 (2014). https://doi.org/10.1371/journal.pone.0085678.
33. E.A. Hussein, I.M. Shaheed, R.S. Hatam, M.M. Kadhim, D.T. Al-kadhum, Adsorption, Thermodynamic and DFT Studies of Removal RS Dye on the Iraq Clay from Aqueous Solutions, 11 (2020) 495–502. https://doi.org/10.5530/srp.2020.3.63.

34. Li H, Leung KS, Ballester PJ, Wong MH. Istar: A web platform for large-scale protein-ligand docking. PLoS One. 2014;9(1).
35. Mustafa M.K., AbbasW.S., Ameerah M. Z., and Wesam R.K., Inhibition of SARS-CoV-2 reproduction using Boswellia carterii: A theoretical study. J. of Mole. Liq. 337 (2021) 116440